

Compositionally graded ferroelectric multilayers for frequency agile tunable devices

C. V. Weiss¹, M. B. Okatan¹, S. P. Alpay¹,
M. W. Cole², E. Ngo², R. C. Toonen²

Received: 23 March 2009 / Accepted: 22 April 2009 / Published online: 8 May 2009
Springer Science+Business Media, LLC 2009

Abstract Recently, there has been significant interest in tunability of BST multilayers. Experimentally, compositionally graded BST multilayers (5 mol% MgO doped and voltage-controlled, frequency-agile phase shifters and resonators) were grown via metallo-organic solution deposition operating in the microwave regime. The fundamental challenge in designing materials systems for such tunable devices is the simultaneous requirement of high dielectric tunability (40%) over a large temperature interval nominal thickness with compositions corresponding to $\text{Ba}_{0.60}\text{Sr}_{0.40}\text{TiO}_3$ (BST 60/40), BST 75/25, and BST 90/10. We show that a high- and temperature-insensitive tunability of 0.012 and a dielectric tunability of 65% at 444 kV/cm. can be realized in compositionally graded ferroelectrics and these properties exhibit minimal dispersion as a function of temperature ranging from 90 to -10 °C. Our results also provide a brief review of the results of experimental and theoretical studies on the dielectric properties of Barium Strontium Titanate ($\text{Ba}_x\text{Sr}_{1-x}\text{TiO}_3$ or BST) multilayer heterostructures. Theoretically, we discuss the role of thermal stresses on the dielectric properties using a non-linear thermodynamic model coupled with basic electrostatic considerations to describe the interlayer interactions between the ferroelectric layers. We show that the thermal tunability, and the loss characteristics for graded undoped BST are 261, 25% (at 1,778 kV/cm), and 0.078, respectively, and 189 and 15% (at 1,778 kV/cm), and 0.039, have a significant effect on the dielectric permittivity and respectively, for the MgO-doped graded BST.

C. V. Weiss · M. B. Okatan · S. P. Alpay (✉)
Materials Science and Engineering Program and Institute
of Materials Science, University of Connecticut, Storrs,
CT 06269, USA
e-mail: p.alpay@ims.uconn.edu

M. W. Cole · E. Ngo · R. C. Toonen
Weapons and Materials Research Directorate, Active Materials
Research Group, U.S. Army Research Laboratory,
Aberdeen Proving Ground, MD 21005, USA

M. W. Cole
e-mail: mcole@arl.army.mil

Introduction

Non-linear dielectric materials are promising candidates for use in a variety of tunable devices, such as phase shifters, tunable filters, delay lines, and oscillators because the dielectric response of the material can be adjusted or "tuned" with the application of an external electric field [1, 2]. Ferroelectric (FE) materials are well-known for their strong non-linear response to an applied electric field, both

in the paraelectric and ferroelectric states. In the FE state, in addition to the non-linear response, the polarization also displays hysteretic behavior due to polarization switching. Therefore, research for materials to be used in tunable devices has focused on FE materials in their paraelectric state. One of the leading material candidates for tunable ferroelectrics is Barium Strontium Titanate ($Ba_{1-x}Sr_xTiO_3$ or BST). In BST, the phase transition temperature or the Curie temperature (T_C) which indicates the onset of ferroelectric behavior can be adjusted by varying the relative amounts of barium and strontium content. The T_C for pure barium titanate (BaTiO₃ BTO) is ~ 120 °C, but by adding strontium titanate (SrTiO₃ STO) to make the solid solution BST, T_C can be decreased. For example, $Ba_{0.70}Sr_{0.30}TiO_3$ (BST 70/30) has T_C of ~ 34 °C and for BST 60/40 $T_C \sim 5$ °C [48]. The ability to tailor T_C by controlling the composition is one of the most promising aspects of using BST in different types of tunable electronic devices since the dielectric permittivity and tunability can be maximized in the vicinity of the FE to paraelectric phase transformation. There are several comprehensive reviews on tunable materials, loss mechanisms, device configurations, and specifically BST thin films for tunable device applications [2, 9, 10].

Although BST is a very promising material system to be employed in tunable devices, many limitations of the materials still exist. In order to be utilized in tunable devices, a material must have a high tunability (typically above 40%), a low loss tangent, temperature stability, and all of these properties must be maintained in the microwave range of frequencies (300 MHz to 300 GHz). Furthermore, the high dielectric response and tunability of bulk or single-crystal BST cannot be realized in thin film systems. These strains are caused by many factors including the lattice mismatch between the film and substrate if the films are epitaxial, the difference in coefficients of thermal expansion (CTE) for the film and substrate, the self-strain of the FE phase transformation if the material is grown above the phase transformation temperature, and microstrains due to defects such as dislocations and vacancies [4, 15]. For example, the relative dielectric constant for bulk BST 70/30 can be greater than 10,000 near T_C , while a BST film (thickness ~ 200 nm) of the same composition is predicted to have a dielectric constant of about 300 near T_C [16].

In addition to the internal stresses, the dielectric properties such as tunability and loss are also highly temperature dependent in BST thin films. Temperature stability is crucial for the application of BST in tunable devices for telecommunication applications because these systems will be operated in a large range of temperatures (typically - 10 °C to 90 °C). Recently, much research has been

devoted to graded FE films to control the strains in the thin film structure and consequently improve the dielectric properties and temperature stability. Our theoretical results indicate that the tunability of graded multilayer FEs can be maximized by optimizing the internal electric fields that arise between layers due to the polarization mismatch and the magnitude of the in-plane strains, such heterostructures may also display relatively temperature insensitive dielectric response and tunability.

Although many FE materials may exhibit high tunabilities, the dielectric loss is still quite high for use in many types of microwave tunable devices. One method that has been identified to improve the loss of these materials is through acceptor doping. Dopants (such as Ni^{2+} , Al^{3+} , Ga^{3+} , Mn^{2+} , Fe^{2+} , Fe^{3+} , Mg^{2+} , etc.) typically occupy the B-site of the ABO₃ perovskite structure, substituting for Ti ions. The charge difference between the dopant and the Ti ion can effectively compensate for oxygen vacancies and may decrease dielectric losses [19]. For example, dielectric constant, loss tangent, and tunability (at 237 kV/cm) of BST 60/40 for 5 mol% MgO-doped BST 60/40 thin films were reported as 720, 0.1, 28%, and 334, 0.007, 17.2%, respectively [20]. Among all the doping elements used with BST

and other ferroelectric materials, MgO has been identified as one of the most promising candidate for lowering the loss, and thus we will focus on the effect of MgO addition to the dielectric tunability [20, 21].

Since compositionally graded FE films can improve the dielectric response of the thin film over a large temperature range and acceptor doping has been shown to lower dielectric loss, MgO doping combined with compositionally graded FE multilayers presents an opportunity to enhance material properties for tunable devices that require high tunability, low loss, and temperature insensitivity. In this article, we summarize the findings of our recent theoretical and experimental work that incorporates the above-mentioned approaches to improve the dielectric properties of BST thin films. The next section contains a thermodynamic model that provides quantitative results for graded BST tri-layer heterostructure and the substrate. We calculate the dielectric properties and tunability of such multilayers as a function of the CTE of the substrate, the processing temperature, the applied electric field, and the operation temperature. The

Experimental: multilayer section concentrates on the deposition of graded BST multilayer films, microstructural characterization, and measurement of the dielectric properties. In the **Experimental: MgO-doped multilayer films** section, we discuss the role of acceptor doping and graded films on the dielectric response and tunability of multilayer BST films at microwave frequencies.

Thermodynamic theory of graded multilayer FE flms: thermal stresses

organic chemical vapor deposition (MOCVD), the temperature of interest is the flm annealing temperature. It is therefore crucial to understand the degree by which the

Understanding the role of internal stresses on the functional properties of FE thin flms is crucial to tailor the tunability of material properties for different tunable device requirements. It is now well understood that the substrate-induced in-plane strain has a strong influence on the ultimate phase stability of a FE flm. Particularly in the case of epitaxial, single-crystalline systems, recent developments demonstrate that it is possible to create FE phases that may not be found in the single-crystal or bulk parent compound under ambient conditions. Examples include strain-induced ferroelectricity at room temperature in the incipient FE STO, strain-induced ferroelectricity at room temperature of BST 60/40 thin flms with Strontium Ruthenate (SrRuO₃ or SRO) electrodes [23], and rotational phases in ultra-thin PbTiO₃ (PbTiO₃) [24]. These observations are supported by theoretical studies that predict unconventional phases under large mechanical strains, in particular, for in-plane tensile strains. Studies show that compressive strains (in the plane of the flm-substrate interface) may enhance the tetragonal out-of-plane polarization [25, 26], while in-plane tensile strains induce in-plane rotational phases of the polarization. [24] These developments have been reviewed recently by Schlom et al [27]. Furthermore, FE flms may also exhibit a complex defect microstructure, which may include features such as twins (or poly-domains) [28], in-plane atomic ordering [29], interfacial misfit dislocations (MDs) [30], and threading dislocations (TDs) [31–34]. The evolution of this complicated microstructure is in direct response to the internal stresses that develop during flm growth and subsequent cooling from the deposition and processing temperatures.

thermal strains alter the dielectric response and its We begin our analysis by assuming a [001]-textured flm (along the z-direction, see schematic drawing in Fig. 1). This texture is chosen to isolate the effects of the thermal strains from strain arising from lattice mismatch. The free energy density of each layer in its bulk form can be expressed through a Landau expansion of the form:

$$F(P, T) = F_0 + \frac{1}{2}aP^2 + \frac{1}{4}bP^4 + \frac{1}{6}cP^6 \tag{1}$$

where F_0 is the free energy density of the reference polarization-free paraelectric state above T_C , P is the polarization, and a , b , and c are the dielectric stiffness coefficients. The temperature dependence of the coefficient a is given by the Curie-Weiss law such that $a = (T - T_C)/\epsilon_0 C$, where ϵ_0 is the permittivity of free space, and T_C and C are the Curie temperature and constant, respectively.

In the case of a thin flm of a FE clamped by a thick substrate, there exists a biaxial in-plane stress due to the thermal stresses that arise as the material is cooled down from a processing temperature T_A . Considering the mechanical boundary conditions (equal in-plane stresses and the flm being traction-free in the z-direction), a straightforward Legendre transformation results in renormalized Landau coefficients. Using these boundary conditions and the short-circuit conditions illustrated in Fig.

the free energy functional for a multilayered FE flm as a function of thermal stresses becomes [37]

Since all the flms and heterostructures have to be processed at elevated temperatures (typically 500–800°C), the CTE mismatch between the flm and the substrate becomes a significant parameter that may by itself have a tremendous impact on the dielectric properties [35]. The strain state in the case of a multilayered FE heterostructure or graded FE flm is also inhomogeneous [36] as a position-dependent internal in-plane strain arises from thermal stresses resulting from cooling down from the deposition temperature or the annealing temperature. The reference temperature that determines the thermal strain depends on what is chosen as the processing technique. For physical vapor deposition methods such as pulsed laser deposition (PLD), the critical temperature is the temperature of the substrate during deposition (T_d). For chemical deposition techniques such as spin coating, dip-coating, or metallization

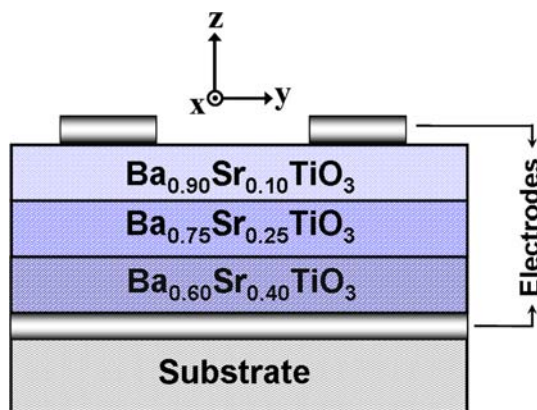


Fig. 1 Schematic diagram of the graded trilayer BST thin flm, including a view of the top and bottom electrodes

$$F_{\Sigma} = \sum_{i=1}^n \alpha_i \left[F_{0,i} + \frac{1}{2} a'_i P_i^2 + \frac{1}{4} b'_i P_i^4 + \frac{1}{6} c_i P_i^6 - E^{\text{ext}} P_i + \frac{x_i^2}{s_{11,i} + s_{12,i}} \right] - \frac{1}{2} \sum_{i=1}^n \alpha_i E_{D,i} P_i \quad (2)$$

in which

$$a'_i = a_i - x_i \frac{4Q_{12,i}}{s_{11,i} + s_{12,i}} \quad (3)$$

$$b'_i = b_i + \frac{4Q_{12,i}^2}{s_{11,i} + s_{12,i}} \quad (4)$$

$$x_i = \int_{T_A}^{T_f} (\lambda_s - \lambda_i) dT \quad (5)$$

$$\sum_{i=1}^n \alpha_i E_{D,i} P_i = -\frac{1}{\epsilon_0} \sum_{i=1}^n \alpha_i (1 - \alpha_i) P_i^2 + \frac{2}{\epsilon_0} \sum_{i=1}^{n-1} \left[\alpha_i P_i \left(\sum_{j=i+1}^n \alpha_j P_j \right) \right] \quad (6)$$

where α_i is the volume fraction of layer i , Q_{mni} and s_{mni} are the electrostrictive coefficients and elastic compliances of layer i , respectively, x_i is the thermal strain in layer i that results from cooling from a high processing temperature T_f to the operation temperature T_A , due to the mismatch between the CTEs of the substrate and layer i . E^{ext} is the externally applied electric field. The electrostatic interlayer interaction is established through the depolarizing field $E_{D,i}$ in layers i that follows from the short-circuit conditions:

$$\sum_{i=1}^n \ell_i E_{D,i} = 0 \quad i = 1, 2, \dots, n \quad (7)$$

$$(P_i - P_{i+1}) + \epsilon_0 (E_{D,i} - E_{D,i+1}) = 0 \quad i = 1, 2, \dots, (n - 1) \quad (8)$$

where ℓ_i is the thickness of layer i . The above set of relations yield the depolarizing field in each layer as:

$$E_{D,i} = -\frac{1}{\epsilon_0} \left(P_i - \sum_{j=1}^n \alpha_j P_j \right) \quad (9)$$

where

$$\alpha_i = \frac{\ell_i}{\sum_{k=1}^n \ell_k} \quad (10)$$

The equilibrium polarizations in the individual FE layers (P_i) follow from the simultaneous solution of the equations of state, $\partial F_{\Sigma} / \partial P_i = 0$. This results in a system of equations for the layers $i = 1, 2, \dots, n$ given by:

$$\alpha_i \left[a_i P_i + b_i P_i^3 + c_i P_i^5 - \frac{4Q_{12,i}}{s_{11,i} + s_{12,i}} P_i x_i - Q_{12,i} P_i^2 + \frac{1}{\epsilon_0} \left(P_i - \sum_{j=1}^n \alpha_j P_j \right) - E^{\text{ext}} \right] = 0 \quad (11)$$

Following the calculation of P_i , the relative small-signal average dielectric response of a perfectly insulating multilayer can be determined from

$$\langle \epsilon \rangle \cong \frac{1}{\epsilon_0} \frac{d\langle P \rangle}{dE} \quad (12)$$

where

$$\langle P \rangle = \sum_i \alpha_i P_i \quad (13)$$

is the average polarization. The dielectric tunability of the multilayer heterostructure at a particular temperature can then be calculated as the change in the average dielectric constant at an applied electric field E^{ext} , with respect to the average dielectric constant at zero applied field;

$$\% \Delta \epsilon = \frac{(\langle \epsilon \rangle @ E = 0 \text{ V/m, } T) - (\langle \epsilon \rangle @ E, T)}{(\langle \epsilon \rangle @ E = 0 \text{ V/m, } T)} \times 100 \quad (14)$$

For the numerical analysis, we consider a trilayer-graded BST heterostructure as shown in Fig. 1. It consists of three layers of equal thickness with compositions corresponding to $\text{Ba}_{0.90}\text{Sr}_{0.10}\text{TiO}_3$ (BST 90/10), BST 75/25, and BST 60/40. We assume that in each layer the thermodynamic parameters (the Curie temperature, Curie constant, dielectric stiffness coefficients, electrostrictive coefficients, elastic compliances, and CTEs) are a linear function of the composition and may be determined by averaging the corresponding values for BTO and STO [5, 22]. CTEs of each layer were assumed to be independent of temperature.

First, we examine the average polarization at room temperature of the trilayer BST structure as a function of the CTE of the substrate and the annealing temperature. Our results show that there is the same trend for all the annealing temperatures in the range of 550–750 °C: below a certain CTE value ($10.29 \times 10^{-6} \text{ K}^{-1}$), the BST multilayer is not spontaneously polarized. In other words, the large in-plane stresses that develop in cooling from a high annealing temperature suppress ferroelectric behavior on substrates with a CTE less than this critical value. These substrates include STO, lanthanum aluminate (La_2AlO_4), and sapphire (Al_2O_3). It is also important to note that if the CTE of the trilayer BST is less than that of the substrate, there are in-plane compressive strains that balance the additional contributions to the free energy from

the electrostatic field due to the (initial) polarization mis-tunability is plotted in Fig. 2c. The average dielectric match between the compositional layers [16]. In this case, permittivity decreases monotonically above and below the critical CTE value of the substrate. For a particular CTE at polarization, and thus ferroelectricity.

Figure 2a and b plot the calculated average dielectric permittivity at room temperature ($R \approx 25^\circ\text{C}$) of the BST multilayer at an applied electric field of 0 kV/cm and 400 kV/cm, respectively. The corresponding dielectric

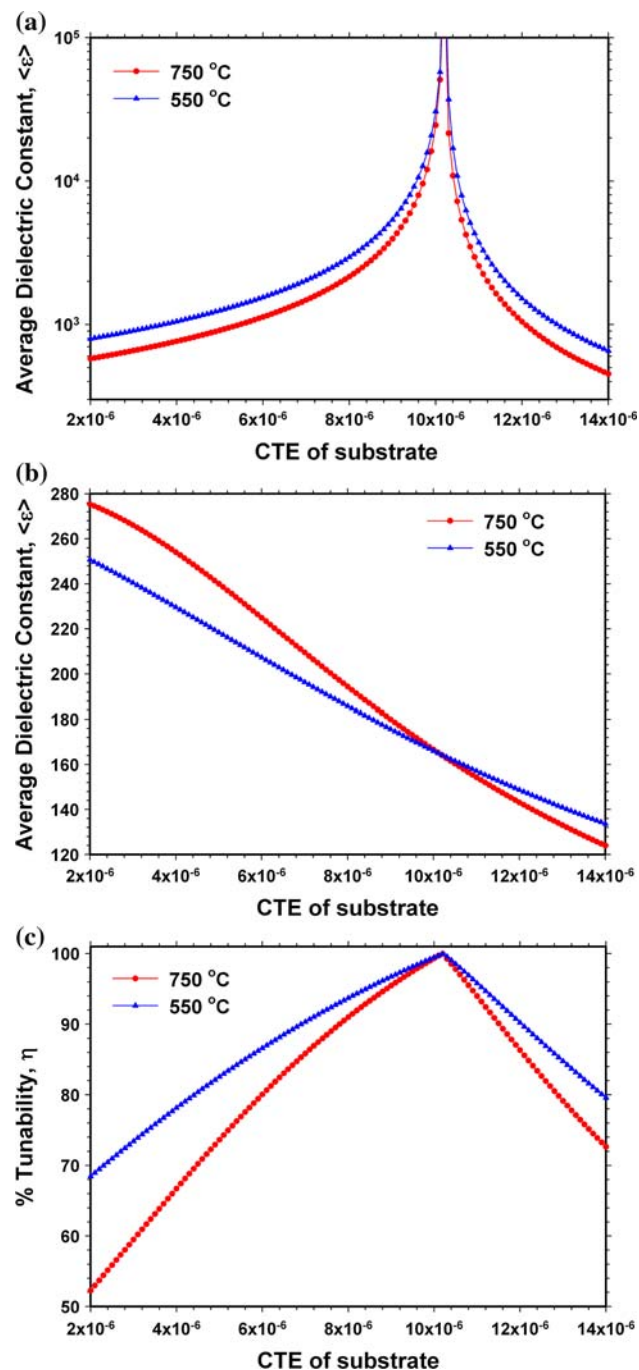


Fig. 2 Dielectric constant of the BST trilayer at $E = 0$ kV/cm and b $E = 400$ kV/cm; c tunability of the BST trilayer at $E = 400$ kV/cm

response increases as the annealing temperature is lowered. On the other hand, when an external electric field of 400 kV/cm is applied, the permittivity increases with increasing annealing temperature and decreases with increasing annealing temperature for PLMs under biaxial compressive stresses. In Fig. 2c, the tunability of the BST multilayer PLM is shown; it exhibits a maximum that is close to 100% at the critical CTE value of the substrate. The tunability increases as the annealing temperature is lowered for both stress states below and above the critical CTE.

In Fig. 3, we show a three-dimensional (3D) plot to demonstrate the effect of varying the temperature and the applied electric field on the tunability of the trilayer BST PLM deposited on Si with $T_A = 750^\circ\text{C}$. As the electric field is increased at a given temperature, the tunability increases reaching a value of 65% at an applied electric field of 400 kV/cm, measured at room temperature (25 °C). The tunability can be further increased by lowering the temperature, with a maximum tunability of 75% at -50°C and a field of 400 kV/cm. Overall, we note that by decreasing the temperature and increasing the applied field, the tunability can be increased significantly. However, this also indicates that the tunability of such trilayer BST devices will be lower at smaller applied fields (which are desired to minimize power usage) and higher temperatures (including those temperatures where tunable devices operate). Future work in this field will undoubtedly focus on maintaining a high tunability (and simultaneous low loss) at lower applied fields, high temperatures, and at microwave frequencies, which will be discussed in the final section.

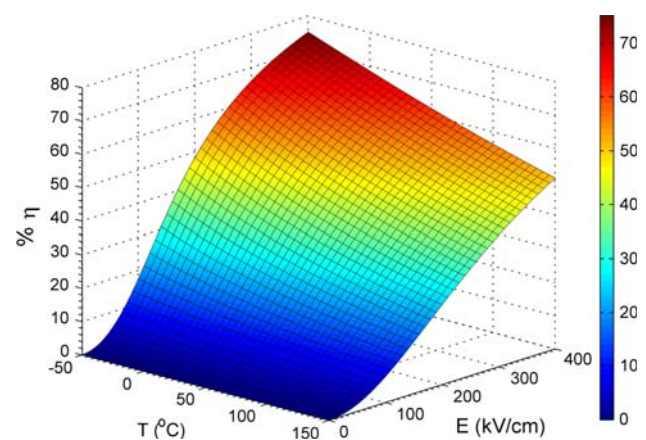


Fig. 3 A 3D plot showing the tunability of the trilayer BST thin PLM as a function of the temperature and the applied electric field, on a Si substrate ($T_A = 750^\circ\text{C}$)

Experimental: multilayer PImS

BST is currently fabricated through a variety of techniques, including sputtering [38], PLD [39], sol-gel [40], polymeric precursor methods [41], and others. Metallo-organic solution deposition (MOSD) can produce extremely uniform PImS since the mixing occurs at the molecular level. The MOSD is also an affordable technique for depositing on large-area substrates with precise control of the stoichiometry and viscosity of the BST precursor solution. Multilayered BST thin PImS were fabricated via MOSD using barium acetate, strontium acetate, and titanium isopropoxide as the precursor materials and glacial acetic acid and 2-methoxyethanol as the solvents. First, barium acetate and strontium acetate were dissolved in glacial acetic acid and the solution was stirred for 1 h until it was clear. Then, the titanium isopropoxide was dissolved in 2-methoxyethanol, and this was added to the barium/strontium solution. The solution was stirred for an additional hour. The precursor solution was spin-coated onto Pt/Si substrates, and particulates were removed from the solution using 0.2- μ m syringe filters. 2-methoxyethanol was added to the solution as needed to adjust the viscosity (and hence the thickness of each spun-on layer) [21, 42]. After the deposition of each layer, the PImS were pyrolyzed on a hot plate at 350 C for 10 min in air to remove any organic addenda. This process was repeated until PImS of approximately * 225-nm thickness were produced. After the deposition of each compositional layer, the PImS were annealed at 750 C for 1 h in flowing oxygen. This multi-annealing protocol was used because it has been shown that annealing procedure helps to minimize the interdiffusion that would take place between the layers if only one annealing step was used [43]. Although a low annealing temperature is beneficial in terms of reducing the thermal stresses, BST thin PImS processed at 750 C have been shown to have high-quality crystalline microstructures [44]. The PImS consist of three compositional layers of BST: BST60/40, BST75/25, and BST90/10, as shown in Fig. 1 and described in the theoretical framework. A uniform composition PIm of the same thickness, corresponding to BST60/40 was also fabricated to compare the effect of the multilayers on the microstructure and dielectric properties. The thin PImS were characterized by X-ray diffraction (XRD), field emission scanning electron microscopy (FESEM), atomic force microscopy (AFM), and dielectric/electrical measurements.

Since the theoretical results indicate that a higher processing temperature often degrades the dielectric properties due to the large thermal strains, we choose the lowest annealing temperature that fully crystallizes the BST and produces a well-formed, defect-free microstructure (750 C). In [thermodynamic theory of graded multilayer](#)

[Fe PImS: thermal stress](#) section, the importance of the CTE mismatch of the substrate and the BST PIm was demonstrated, and it was found to play a significant role in determining the dielectric properties. In the experimental synthesis, we used Si substrates. Although the CTE mismatch between Si and BST layers is relatively large (* 7.9 $\times 10^{-6}$ K⁻¹ for BST60/40 and Si at room temperature) [37], metallized Si is required as a substrate so that the tunable device is compatible with the existing integrated circuit (IC) technology. While other substrates may produce better dielectric properties, Si was chosen partly because of its affordability and compatibility with current microelectronic systems. Much of this research in the field of FE thin PImS focuses on optimizing and integrating other substrates into the IC architecture, and it will likely be focus of future research as well.

A cross-sectional FESEM image is given in Fig. 4. This image demonstrates that the PImS possess a dense, randomly oriented, polycrystalline microstructure with a thickness of * 225 nm. We also note that there is a clear delineation between the bottom Pt electrode and the BST PIm, promoting good contact properties. Furthermore, the FESEM image shows that there are no visible interfaces between the BST layers of different composition. The AFM micrographs are given in Fig. 5. The AFM micrographs verify that the PImS have a dense polycrystalline structure with no observable pinholes or other surface defects. In addition to obtaining AFM images, we also measured the roughness of the BST PImS. Low surface roughness is crucial if the PImS are to be integrated in these devices, because an overly rough surface can cause bad contact between the PIm and top electrode and this promotes high conductor loss. A smooth PIm (roughness * 5 nm) promotes better contact properties between the PIm and electrode, thereby lowering the leakage current and overall insertion loss and providing long-term reliability in the device structure. The roughness of the

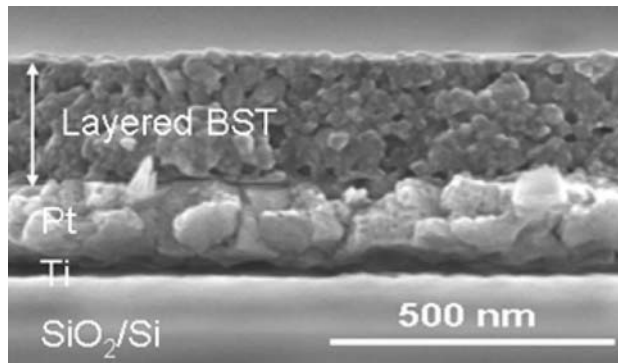
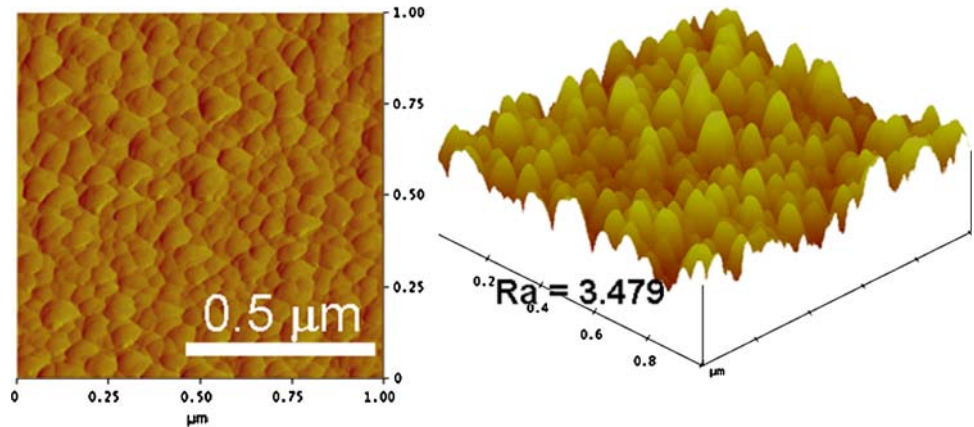


Fig. 4 Cross-sectional FESEM image showing the undoped trilayer BST thin PIm on the Pt/Si substrate (Reprinted with permission from American Institute of Physics, Copyright 2007)

Fig. 5 Plan-view and cross-sectional AFM images of the undoped trilayer BST thin film, demonstrating the dense grain structure and low surface roughness (Reprinted with permission from American Institute of Physics, Copyright 2007)



multilayer films was found to be 3.5 nm, which is well within the acceptable range for tunable devices. This surface roughness value is comparable to roughness values found in uniform film BST thin films fabricated by the same method.

X-ray diffraction results are given in Fig. 6. In general, the XRD data confirm that the films have a polycrystalline perovskite structure (of the form AB_3O_7). No secondary phases are present in the film. In comparing the XRD data for the uniform BST60/40 film and the graded (or up-graded) BST film, we see a slight downshift in peak positions for the graded film. This downshift may be attributed to the larger lattice parameter in the multilayer films, which is caused by the increase in lattice parameter as the Ba/Sr ratio increases. Since the lattice parameter of the multilayer film is an average of the lattice parameters of each of the layers, the increasing Ba/Sr ratio in the film causes a larger average lattice parameter, and hence the XRD peak shifts downward. The increase in lattice parameter may also arise from the cooling of the films from a high annealing temperature, since interface defects and thermal strains may develop in the film as it is cooled, as described earlier. In fact, the surface roughness value is comparable to roughness values found in uniform film BST thin films fabricated by the same method. In fact, the surface roughness value is comparable to roughness values found in uniform film BST thin films fabricated by the same method.

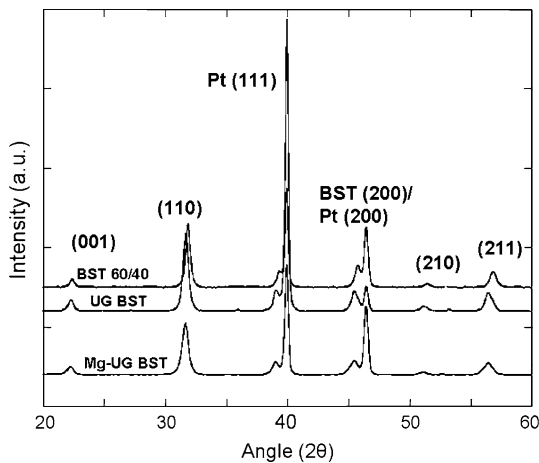


Fig. 6 X-ray diffraction patterns of the uniform BST60/40 film (top), the multilayer up-graded BST film (middle), and the MgO-doped multilayer UG BST films as a function of temperature (Reprinted with permission from American Institute of Physics, Copyright 2008)

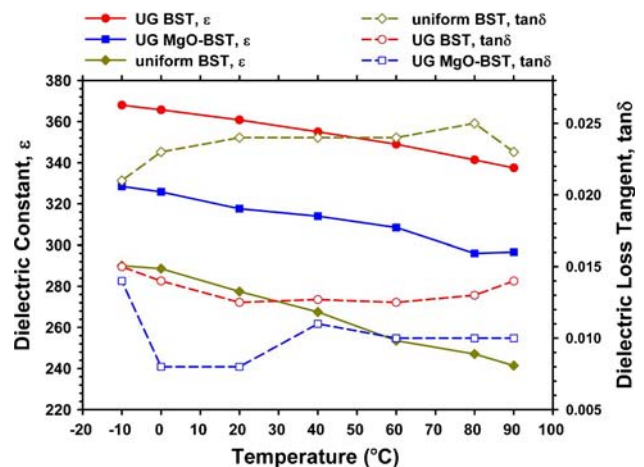


Fig. 7 The dielectric constant and loss tangent of uniform composition BST, undoped multilayer upgraded (UG) BST films, and MgO-doped multilayer UG BST films as a function of temperature (Reprinted with permission from American Institute of Physics, Copyright 2008)

temperature range of 10 °C to 90 °C in the multilayer construct. There is no evidence of anomalous peaks, which often indicate the phase transition temperature of one of the multilayer compositions [39]. The multilayer BST PIm possessed both a higher permittivity ($\epsilon = 364$) and lower loss ($\tan \delta = 0.012$) than the uniform BST60/40 PIm ($\epsilon = 280$ and $\tan \delta = 0.023$) at room temperature. Although the composition BST60/40 has a Curie temperature just below room temperature (6), making it paraelectric at room temperature, the compositions of BST75/25 and BST90/10 have different T_c values as discussed earlier, and they have higher permittivity values which increase the average dielectric response for the multilayer PIm construct. Also, higher permittivity in the multilayer PIm may be influenced by the electrostatic reaction between different compositional layers. Figure 7 also verifies the theoretical results given in Fig. 6 mainly that in the graded multilayer PIm, the dielectric response increased as the temperature decreased. Overall though, the multilayer structure produced mostly temperature insensitive behavior in the range 10 °C to 90 °C, as predicted by the thermodynamic model.

The loss tangent for the multilayer PIm is lower than that of a uniform composition PIm, and it is also quite low compared to many results in the literature, including graded PIm made by sol-gel, PLD, and other methods [46]. However, dielectric loss values for graded BST thin PIm span a large range in the experimental literature, most likely due to the differences in crystalline quality, defect concentration, and thermal and mechanical strains that arise during thin PIm deposition and processing [47, 48]. Although the increase in permittivity values in multilayered PIm can be attributed to the presence of ferroelectric layers and interlayer electrostatic coupling, the lower loss values in multilayered PIm is not as well understood. The lower loss tangent in multilayered PIm may be due to the fact that defects are trapped at the compositional interfaces and are no longer mobile enough to reach the electrodes and contribute to the loss mechanism.

The tunability of the multilayered BST compared to the uniform BST thin PIm is given in Fig. 8. Here, we see an increase of $\sim 56\%$ in the tunability for the trilayer PIm as compared to the uniform composition BST thin PIm, due to the increase in the permittivity in the multilayer PIm as discussed above.

Experimental: MgO-doped multilayer PIm

Doping BST PIm with MgO has been determined as one of the ways to lower the loss tangent. Therefore, combining acceptor doping with a multilayered PIm design can help lower loss, while simultaneously maintaining a high

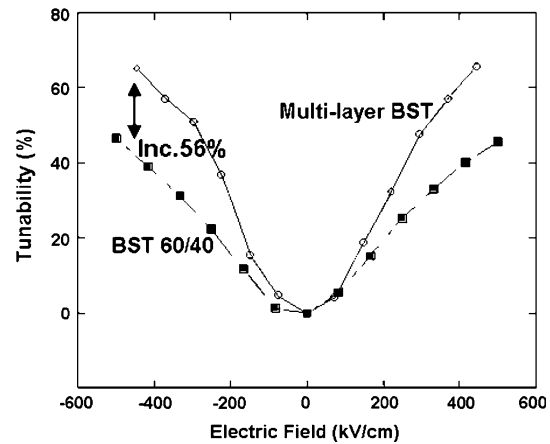


Fig. 8 Tunability at room temperature of the uniform BST60/40 PIm (filled squares) and the trilayer BST thin PIm (open circles) as a function of the applied electric field (Reprinted with permission from American Institute of Physics, Copyright 2007)

permittivity and tunability over a wide temperature range. The same experimental procedure and device design described above were used to make the BST PIm, except that in this case, each compositional layer is MgO-doped BST. We will compare the doped multilayered PIm to that of an undoped multilayer BST PIm, and a uniform composition BST60/40 PIm. As in the case for the undoped multilayer PIm, XRD, AFM, and FESEM results indicate that the PIm has a dense, well-crystallized microstructure with randomly oriented grains and no defects or secondary phases. Compared to some other experimental results involving MgO-doping of BST, our XRD results indicate an enhanced degree of solubility of the MgO. This enhanced solubility is most likely due to the mixing at the molecular level that occurs in the MOSD process, as well as the induced thermal strains discussed previously [49]. Here, we chose 5 mol% MgO doping because it has been shown that a concentration in excess of 10 mol% creates a PIm that is no longer a single phase [21]. In addition to the increase in lattice parameter that was observed in the multilayer structure, we also get an additional increase in the lattice parameter due to the MgO doping. Since Mg has a larger ionic radius than Ti (0.072 nm compared to 0.061 nm), the addition of MgO into the lattice actually causes the lattice to expand slightly, which we can observe in the XRD data in Fig. 6. The AFM micrographs indicate that the doping of BST with MgO produced a smaller grain size (60 nm vs. 72 nm for the undoped multilayer PIm). This smaller grain size caused a decrease in the overall surface roughness as well (3.1 nm vs. 3.5 nm for the undoped multilayer PIm). Overall, MgO doping of multilayer PIm causes enhanced material properties, such as lower surface roughness, and maintains the desirable microstructure for BST in tunable devices.

Figure 7 shows the permittivity and loss for the MgO-doped multilayered PIm as a function of temperature. We see that the permittivity and loss are both very stable as function of temperature from 10 °C to 90 °C, as expected from the graded multilayer PIm design. The doped, multilayer PIm has a lower loss than the undoped multilayer PIm (0.010 at 90 °C compared to 0.014 for the undoped multilayer PIm at 90 °C), but the MgO-doped PIm also has a lower dielectric constant (330 at 10 °C compared to 370 for the undoped multilayer PIm at 10 °C). Even though the MgO-doped graded PIm has a lower permittivity, the low loss and temperature stability are promising results for the use of MgO doping and compositional grading in temperature-stable tunable devices.

Since the doped multilayer PIm have been shown to possess very low loss (due to the MgO doping) and exceptional temperature stability (due to the compositional grading), we now will examine the dielectric properties (permittivity, loss, and tunability) as a function of frequency. Many tunable devices will be operated in the microwave range of frequencies, but we expect that the dielectric properties will degrade at very large frequencies due to relaxation effects caused by the presence of defects [50]. Therefore, we compare the permittivity, loss, and tunability of the undoped and doped multilayer PIm at three frequencies: 0.5 GHz, 5 GHz, and 10 GHz. We expect the MgO doping to have a strong influence on the loss characteristics of the multilayer PIm at high frequencies; however, it is important to note that the permittivity (and hence the tunability, given by Eq. (3), is closely related to the loss tangent. For example, even though acceptor doping has been shown to decrease loss in BST

thin PIm, it has also been shown to decrease the permittivity and tunability. In determining the best PIm characteristics (such as the strength of the composition gradient, the number of compositional layers, the dopant material, and the doping concentration), we must keep in mind that the simultaneous requirement of low loss and high tunability will ultimately represent a compromise between these two parameters.

Figure 9 shows the variation in the permittivity with the applied field for (a) the trilayer BST PIm and for (b) the MgO-doped trilayer BST PIm at microwave frequencies. As expected, doping with MgO lowers the permittivity of the trilayer structure at all the applied frequencies. This phenomena can be partly explained by the fact that adding MgO lowers T_C [51]. Also, adding MgO into the BST lattice causes a slight volumetric expansion, as discussed previously [52]. However, we note that as the frequency increased, the permittivity values are fairly constant for the doped PIm, whereas in the undoped PIm, the frequency has

a large effect on the permittivity. Therefore, we expect that acceptor doping might prove to be a useful method to

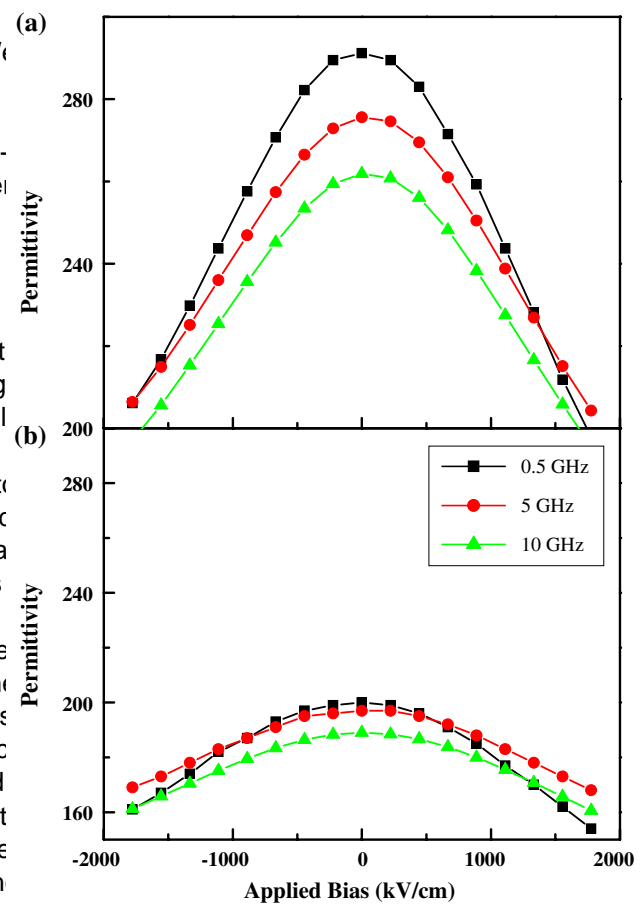


Fig. 9 The permittivity of the undoped multilayer BST PIm and the MgO-doped multilayer BST PIm at 0.5, 5, and 10 GHz frequencies (Reprinted with permission from American Institute of Physics, Copyright 2008)

maintain a nearly constant dielectric response over a large range of frequencies, including microwave frequencies.

In Fig. 10, we have plotted the loss as a function of the applied field for the undoped (a) and doped (b) graded multilayer PIm. For both PIm, we see that increasing the frequency causes an increase in the loss tangent. This

increase in the dielectric loss is most likely due to a number of effects, including quasi-Debye type losses, and losses associated with oxygen vacancies and other defects [53].

However, this increase in the loss is much more pronounced in the undoped PIm, confirming our prediction that doping the trilayer structure with MgO would lower losses at microwave frequencies. Although the loss at microwave frequencies is significantly higher than at lower frequencies (0.008 at 100 kHz for the undoped trilayer PIm, compared to 0.039 at 10 GHz for the doped, trilayer PIm [52]), these loss values are still within the acceptable range for many types of tunable devices.

Figure 11 shows tunability as a function of the applied electric field for (a) an undoped trilayer BST PIm and (b)

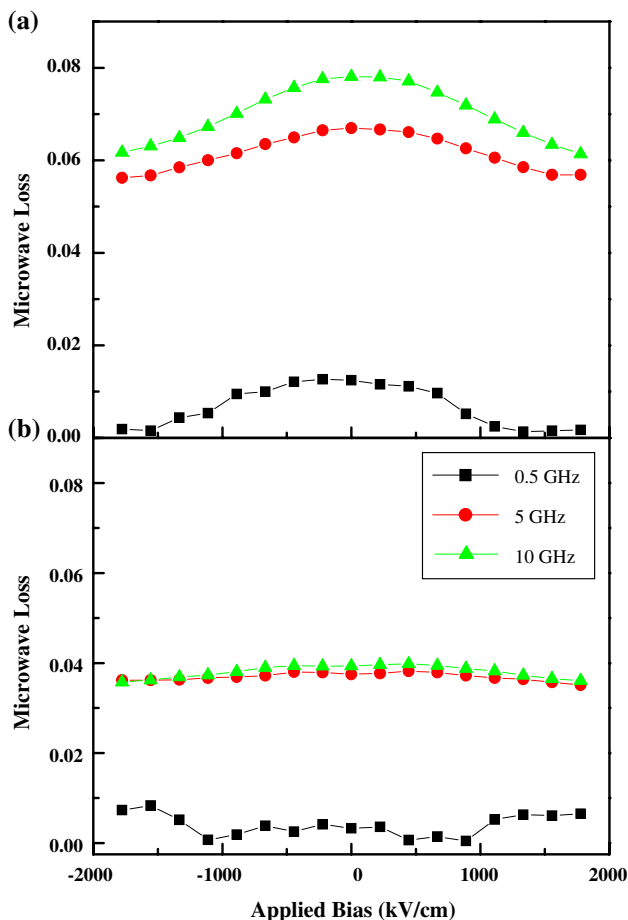


Fig. 10 The microwave dielectric loss tangent of the undoped multilayer BST PIm and the MgO-doped multilayer BST PIm at 0.5, 5, and 10 GHz (Reprinted with permission from American Institute of Physics, Copyright 2008)

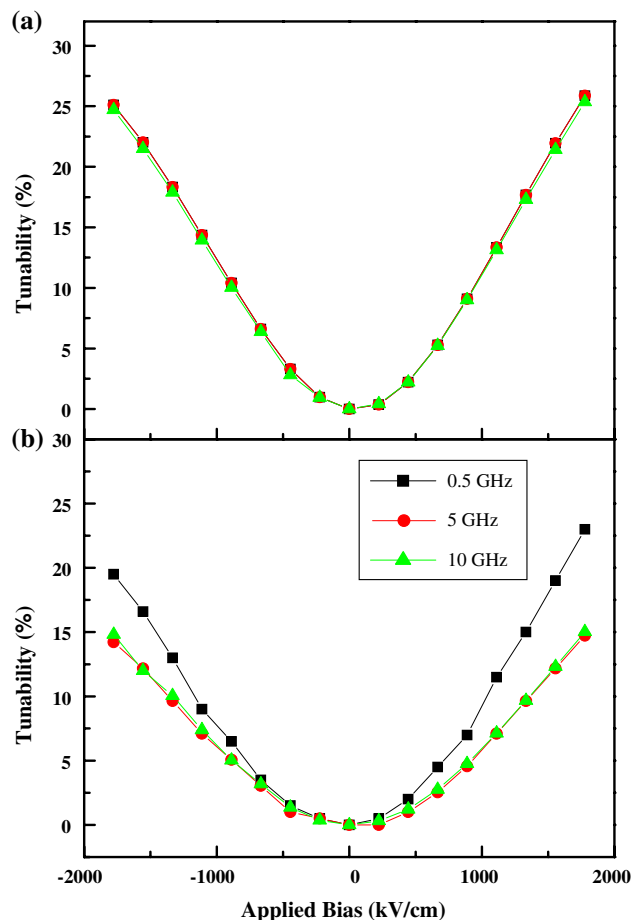


Fig. 11 The tunability of the undoped multilayer BST PIm and the MgO-doped multilayer BST PIm measured at 0.5, 5, and 10 GHz (Reprinted with permission from American Institute of Physics, Copyright 2008)

and MgO-doped trilayer BST PIm. Doping with MgO lowered the tunability, which is related to the decrease in the permittivity discussed above. The MgO doping also caused a larger dispersion in tunability with applied frequency, as compared to the undoped PIm. For example, the tunability of the MgO-doped graded multilayer PIm at 1,778 kV/cm and 10 GHz is 15%, while at the same applied field and 0.5 GHz, the tunability is 20%. For the undoped trilayer PIm, the tunability did not show a significant change with the frequency.

Although compositional grading and acceptor doping have demonstrated excellent dielectric properties in the microwave range of frequencies, many other methods to improve the dielectric properties of ferroelectric thin films over a large frequency and temperature range are currently being investigated. Some of the methods currently being investigated include choosing the appropriate substrate [53] and carefully adjusting the thin film thickness [54]. The theoretical results also indicate that dielectric properties can be improved over a wide temperature range from the CTE mismatch between the PIm and substrate

significantly influence the dielectric permittivity and tunability of BST multilayers. Experimentally, BST compositionally multilayered (5 mol% MgO-doped and undoped) films were fabricated via MOSD on Pt/Si. The best dielectric properties (dielectric permittivity of 360, loss of 0.012, and a tunability of 65% at 444 kV/cm) were found to exist in BST heterostructures consisting of three distinct layers of ~220 nm nominal thickness with compositions corresponding to BST 60/40, BST 75/25, and BST 90/10. These properties exhibited minimal dispersion as a function of temperature ranging from 90°C to -10°C. Although MgO doping improves dielectric loss, it also results in a moderate tunability (29% at 444 kV/cm). Electrical measurements at 10 GHz display a decrease in the dielectric permittivity and tunability for both undoped and MgO-doped BST multilayers.

Acknowledgements This study at UConn was supported by the U.S. Army Research Office through Grants W911NF-05-1-0528 and W911NF-08-C-0124. The authors would like to thank C. Hubbard for the XRD measurements, and S. Hirsch for the SEM analysis.

References

- Lancaster MJ, Powell J, Porch A (1998) *Supercond Sci Technol* 11:1323
- Tagantsev AK, Sherman VO, Astafev KF, Venkatesh J, Setter N (2003) *J Electroceram* 11:5
- Kingery WD, Bowen HK, Uhlmann DR (1976) *Introduction to ceramics*, 2nd edn. Wiley, New York
- Pertsev NA, Zembilgotov AG, Tagantsev AK (1998) *Phys Rev Lett* 80:1988
- Pertsev NA, Tagantsev AK, Setter N (2000) *Phys Rev B* 61:R825
- Landolt H, Bornstein R (1981) *Numerical data and functional relationships in science and technology*. Springer, Berlin
- Yamada T (1972) *J Appl Phys* 43:328
- Hilton AD, Ricketts BW (1996) *J Phys D: Appl Phys* 29:1321
- Bao P, Jackson TJ, Wang X, Lancaster MJ (2008) *J Phys D: Appl Phys* 41:1
- Vendik OG, Hollmann EK, Kozyrev AB, Prudan AM (1999) *J Supercond* 12:325
- Wu L, Wu S, Chang FC, Shen YT, Chen YC (2000) *J Mater Sci* 35:5945. doi:10.1023/A:1026722206381
- Cole MW, Weiss CV, Ngo E, Hirsch S, Coryell LA, Alpay SP (2008) *Appl Phys Lett* 92:182906
- Cole MW, Hubbard C, Ngo E, Ervin M, Wood M, Geyer RG (2002) *J Appl Phys* 92:475
- Ban ZG, Alpay SP (2002) *J Appl Phys* 91:9288
- Ban ZG, Alpay SP (2003) *J Appl Phys* 93:504
- Shaw TM, Suo Z, Huang M, Liniger E, Laibowitz RB, Baniecki JD (1999) *Appl Phys Lett* 75:2129
- Zhong S, Alpay SP, Mantese JV (2006) *Appl Phys Lett* 88:132904
- Cole MW, Joshi PC, Ervin MH (2001) *J Appl Phys* 89:6336
- Podpirka A, Cole MW, Ramanathan S (2008) *Appl Phys Lett* 92:212906
- Cole MW, Nothwang WD, Hubbard C, Ngo E, Ervin MH (2003) *J Appl Phys* 93:9218
- Cole MW, Joshi PC, Ervin MH, Wood MC, Pfeffer RL (2000) *Thin Solid Films* 374:34
- Li YL, Choudhury S, Haeni JH, Biegalski MD, Vasudevarao A, Sharan A, Ma HZ, Levy J, Gopalan V, Trolier-McKinstry S, Schlom DG, Jia QX, Chen LQ (2006) *Phys Rev B* 73:184112
- Qin WF, Ai WY, Zhu J, Xiong J, Tang JL, Zhang Y, Li YR (2007) *J Mater Sci* 42:8707. doi:10.1007/s10853-007-1739-y
- Catalan G, Janssens A, Rispens G, Csiszar S, Seeck O, Rijnders G, Blank DHA, Noheda B (2006) *Phys Rev Lett* 96:127602
- Roytburd AL, Alpay SP, Nagarajan V, Ganpule CS, Aggarwal S, Williams ED, Ramesh R (2000) *Phys Rev Lett* 85:190
- Ederer C, Spaldin NA (2005) *Phys Rev Lett* 95:257601
- Schlom DG, Chen LQ, Eom CB, Rabe KM, Streiffer SK, Triscone JM (2007) *Ann Rev Mater Res* 37:589
- Kwak BS, Erbil A, Budai JD, Chisholm MF, Boatner LA, Wilkens BJ (1994) *Phys Rev B* 49:14865
- Zhang LC, Vasiliev AL, Misirliglu IB, Ramesh R, Alpay SP, Aindow M (2008) *Appl Phys Lett* 93:262903
- Speck JS, Daykin AC, Seifert A, Romanov AE, Pompe W (1995) *J Appl Phys* 78:1696
- Misirliglu IB, Vasiliev AL, Alpay SP, Aindow M, Ramesh R (2006) *J Mater Sci* 41:697. doi:10.1007/s10853-006-6488-9
- Misirliglu IB, Alpay SP, Aindow M, Nagarajan V (2006) *Appl Phys Lett* 88:102906
- Misirliglu IB, Vasiliev AL, Aindow M, Alpay SP, Ramesh R (2004) *Appl Phys Lett* 84:1742
- Vrejoiu I, Le Rhun G, Zakharov ND, Hesse D, Pintilie L, Alexe M (2006) *Philos Mag* 86:4477
- Sharma A, Ban ZG, Alpay SP, Mantese JV (2004) *Appl Phys Lett* 85:985
- Akay G, Zhong S, Allimi BS, Alpay SP, Mantese JV (2007) *Appl Phys Lett* 91:012904
- Okatan MB, Cole MW, Alpay SP (2008) *J Appl Phys* 104:104107
- Tsai MS, Sun SC, Tseng TY (1997) *J Appl Phys* 82:3482
- Lu SG, Zhu XH, Mak CL, Wong KH, Chan HLW, Choy CL (2003) *Appl Phys Lett* 82:2877
- Jain M, Majumder SB, Katiyar RS, Miranda FA, Van Keuls FW (2003) *Appl Phys Lett* 82:1911
- Saravanan KV, Raju KCJ, Krishna MG, Bhatnagar AK (2007) *J Mater Sci* 42:1149. doi:10.1007/s10853-006-1435-3
- Zhu X, Lu S, Chan HLW, Choy CL, Wong KH (2003) *Appl Phys A: Mater Sci Process* 76:225
- Cole MW, Ngo E, Hirsch S, Demaree JD, Zhong S, Alpay SP (2007) *J Appl Phys* 102:034104
- Jiang Q, Gao YH, Cao HX (2004) *Phys Lett A* 331:117
- Tian HY, Luo WG, Pu XH, Qiu PS, He XY, Ding AL (2001) *Solid State Commun* 117:315
- Zhu X, Chan HLW, Choy CL, Wong KH (2002) *J Vac Sci Tech A: Vac Surf Films* 20:1796
- Zhu XH, Chong N, Chan HLW, Choy CL, Wong KH, Liu Z, Ming N (2002) *Appl Phys Lett* 80:3376
- Kim WJ, Chang W, Qadri SB, Pond JM, Kirchoefer SW, Chrisey DB, Horwitz JS (2000) *Appl Phys Lett* 76:1185
- Okhay O, Wu AY, Vilarinho PM (2005) *J Eur Ceram Soc* 25:3079
- Elissalde C, Ravez J (2001) *J Mater Chem* 11:1957
- Su B, Button TW (2004) *J Appl Phys* 95:1382
- Cole MW, Ngo E, Hirsch S, Okatan MB, Alpay SP (2008) *Appl Phys Lett* 92:072906
- Su B, Button TW, Price T, Iddles D, Cannell D (2008) *J Mater Sci* 43:847. doi:10.1007/s10853-007-2216-3
- Weiss CV, Cole MW, Alpay SP, Ngo E, Toonen RC, Hirsch SG, Demaree JD, Hubbard C (2008) *Integr Ferroelectr* 100:36